Tropospheric ozone and nitrogen dioxide measurements in urban and rural regions as seen by IASI and GOME-2

Sarah Safieddine, Cathy Clerbaux, Maya George, Juliette Hadji-Lazaro, Daniel Hurtmans, Pierre-François Coheur, Catherine Wespes, Diego Loyola, Peter Valks, Nan Hao

Tropospheric ozone and nitrogen dioxide measurements in urban and rural regions as seen by IASI and GOME-2

S. Safieddine,[1] C. Clerbaux,[1,2] M. George,[1] J. Hadji-Lazaro,[1] D. Hurtmans,[2] P.-F. Coheur,[2] C. Wespes,[2] D. Loyola,[3] P. Valks,[3] and N. Hao[3]

Received 11 February 2013; revised 31 May 2013; accepted 17 July 2013; published 17 September 2013.

[1] Tropospheric ozone (O_3) columns in urban and rural regions as seen by the Infrared Atmospheric Sounding Interferometer (IASI) are analyzed along with the Global Ozone Monitoring Experiment (GOME-2) tropospheric nitrogen dioxide (NO_2) columns. Results over nine cities of the Northern Hemisphere for the period 2008–2011 show a typical seasonal behavior of tropospheric O_3, with a first maximum reached in late spring because of stratospheric intrusion mainly and a continuous rise till the summer because of the anthropogenic-based ozone production. Over the East Asian cities, a decrease in the O_3 tropospheric column is detected during the monsoon period. Seasonal cycling of tropospheric NO_2 shows consistent higher values during winter because of the higher anthropogenic sources and longer lifetime. In rural regions, a complex relation between the O_3 and NO_2 columns is found, with good correlation in summer and winter. O_3 concentrations in rural sites are found to be comparable to those closest to the anthropogenic emission sources, with peak values in spring and summer. Furthermore, the effect of the reduction of pollutant emissions in the Beijing region during the Olympic Games of 2008 compared to the same summer period in the following 3 years is studied. GOME-2 NO_2 measurements show a reduction up to 54% above Beijing during this period compared to the following 3 years. IASI O_3 measurements show an increase of 12% during July 2008 followed by a decrease of 5–6% during the months of August and September.

Citation: Safieddine, S., C. Clerbaux, M. George, J. Hadji-Lazaro, D. Hurtmans, P.-F. Coheur, C. Wespes, D. Loyola, P. Valks, and N. Hao (2013), Tropospheric ozone and nitrogen dioxide measurements in urban and rural regions as seen by IASI and GOME-2, *J. Geophys. Res. Atmos.*, *118*, 10,555–10,566, doi:10.1002/jgrd.50669.

1. Introduction

[2] Global monitoring of tropospheric O_3 is essential as it is an important greenhouse gas and air pollutant [*Jacobson*, 2012]. It is a significant absorber of infrared and ultraviolet (UV) radiation and a primary source of the most important oxidant in the atmosphere, the hydroxyl radical OH, that is highly reactive with organic and inorganic compounds [*Levy et al*., 1985; *Finlayson-Pitts and Pitts*, 1997; *Jacob*, 2000]. Exposure to high levels of O_3 is associated with pulmonary and chronic respiratory diseases as well as premature mortality [*Bell et al*., 2004, 2007; *Ito et al*., 2005; *Ebi and McGregor*, 2008]. Economic concerns are also raised because of the negative effect of O_3 on vegetation, ecosystems, crops production, and yield [*Reich*, 1983; *Chappelka et al*., 1999; *Collins et al*., 2000; *Fuhrer and Booker*, 2003; *Schaub et al*., 2005; *Karnosky et al*., 2007].

[3] Sources of O_3 in the troposphere are due to either natural intrusion from the stratosphere, where most of the O_3 resides, or photochemical production from precursors. These precursors are pollutants emitted mainly during anthropogenic urban activities and include carbon monoxide (CO), peroxy radicals generated by the photochemical oxidation of the Volatile Organic Compounds (VOCs), such as hydrocarbons and aldehydes, and nitrogen oxides ($NO_x = NO + NO_2$). The main sources of NO_x are either anthropogenic, such as the result of the combustion of fossil fuels and biomass burning, or natural from wildfires, soil emissions, and lighting. Most of the NO_2 in urban air results from the rapid oxidation of NO which is the major nitrogenous product emitted from combustion [*Finlayson-Pitts and Pitts*, 1997; *Klonecki and Levy*, 1997; *Jacob*, 2000; *Seinfeld and Pandis*, 2006; *Jacobson*, 2012]. One can distinguish two regimes with different O_3-NO_x-VOC sensitivity. The first one is the NO_x-limited regime where O_3 concentrations increase with increasing NO_x, and the second one is the VOC-limited (NO_x-saturated) regime, where O_3 production rate increases with increasing VOCs concentrations. Generally, urban centers are found to be in a VOC-limited regime, while rural regions downwind are found to be in a

[1]UPMC Univ. Paris 06; Université Versailles St-Quentin; CNRS/INSU; LATMOS-IPSL, Paris, France.
[2]Spectroscopie de l'Atmosphère, Chimie Quantique et Photophysique, Université Libre de Bruxelles, Brussels, Belgium.
[3]Remote Sensing Technology Institute (IMF), German Aerospace Center (DLR), Oberpfaffenhofen, Germany.

Corresponding author: S. Safieddine, UPMC Univ. Paris 06; Université Versailles St-Quentin; CNRS/INSU; LATMOS-IPSL, 4 place Jussieu, FR-75252 Paris, France. (safieddine@latmos.ipsl.fr)

2169-897X/13/10.1002/jgrd.50669

NO_x-limited regime [*Milford et al*., 1989, 1994; *Sillman*, 1999; *Duncan et al*., 2010]. In fact, O_3 concentrations in rural sites are frequently found to be higher than the values found near anthropogenic activity, with peak values in spring and summer [*Logan*, 1985, 1989; *Sillman et al*., 1990]. The measurement of tropospheric O_3 and NO_2 by satellite is shown to be efficient since it provides a good way to get regional and global information on O_3 and NO_2 distributions, transport, and variability [*Tie et al*., 2007]. Tropospheric O_3 retrievals from satellites have been possible by subtracting the stratospheric O_3 column with UV sounders [e.g., *Fishman and Larsen*, 1987; *Schoeberl et al*., 2007], directly from measurements in the UV [*Liu et al*., 2006], and from high-resolution infrared sounders like the Interferometric Monitor for Greenhouse gases (IMG), the Tropospheric Emission Spectrometer (TES), and IASI [*Coheur et al*., 2005; *Worden et al*., 2007; *Eremenko et al*., 2008].

[4] In this paper we analyze the seasonal variations of O_3 and NO_2 in the troposphere, over 4 years (2008–2011) above specific urban and rural areas of the Northern Hemisphere (NH), using data provided by the IASI and GOME-2 instruments on the MetOp-A (Meteorological Operational) satellite along with wind patterns provided by ECMWF (European Centre for Medium-Range Weather Forecasts) Reanalysis (ERA). Section 2 details the study area selection and how measurements data are collocated above cities. In section 3 we explain the method used to extract wind directions and the tropospheric O_3 retrieval from the IASI mission as well as GOME-2 retrievals of the tropospheric NO_2 columns. We discuss the results in section 4 and list our conclusions in section 5.

2. Study Area Selection

[5] In order to understand the effect of local pollution, we chose to focus in this study on a selected set of big cities, listed in Table 1, known for their high anthropogenic emissions in different locations in the NH and over three continents: North America, Europe, and Asia. Over the period from January 2008 to December 2011, monthly averaged gridded tropospheric O_3 and NO_2 columns were calculated, over a grid size of $0.25° \times 0.25°$. The corresponding rural area for each city was defined as the area downwind the city (see section 3.1).

3. Measurements

[6] High-pollution episodes are notably detected above and around cities. During such events, elevated values of NO_2 and O_3 can be observed by satellite in the troposphere [e.g., *Tie et al*., 2007; *Dufour et al*., 2010]. In this study we aim at investigating the relation between O_3 and NO_2 pollution over cities and their corresponding rural areas using satellite data: We use in particular IASI tropospheric O_3 column and GOME-2 tropospheric NO_2 column data. In addition we use wind fields from ECMWF Reanalysis to locate the rural areas where the formation or transport of O_3 is important.

3.1. Wind Directions

[7] Wind direction patterns used in this study are from the ERA-Interim archive at ECMWF (u and v components of horizontal wind). The data assimilation produces four analyses per day at 00:00, 06:00, 12:00, and 18:00 UTC at 37 pressure levels from 1000 to 1 hPa with a Gaussian grid with a resolution of 0.7° at the equator. Data Services associated with wind data sets apply an interpolation scheme to make it adaptable to requested resolutions and representation forms [*Berrisford et al*., 2009; *Dee et al*., 2011]. In the ERA-Interim database, monthly means of wind direction patterns are interpolated and extracted over a grid size of $0.75° \times 0.75°$. In this study, we attempt to analyze the prevailing wind directions from each studied urban city in Table 1. We averaged monthly wind patterns over the 4 year period of the study in the boundary layer (surface to 750 hPa) where the production and transport of pollutants are the most important. The result is inserted as "rural" region in Table 1.

3.2. IASI Ozone Measurements

3.2.1. Instrumentation

[8] The IASI instrument launched on board the MetOp-A platform on 19 October 2006 is a nadir-looking Fourier transform spectrometer that probes the Earth's atmosphere in the thermal infrared spectral range between 645 and 2760 cm^{-1}, with a spectral resolution of 0.5 cm^{-1} (apodized) and a 0.25 cm^{-1} spectral sampling. Three IASI instruments have been assigned for a span of at least 15 years. The second one was launched on 17 September 2012 on board the MetOp-B, and the third instrument is scheduled for 2016–2017. The IASI footprint is a matrix of 2×2 pixels, each with 12 km diameter at nadir. IASI monitors the atmospheric composition at any location two times per day with a swath width of 2200 km corresponding to a total of 120 views. IASI can as well measure many of the chemical components that play a key role in the climate system and are responsible for atmospheric pollution [*Clerbaux et al*., 2009; *Coheur et al*., 2009; *Turquety et al*., 2009; *Clarisse et al*., 2011]. As far as O_3 is concerned, vertical information has been demonstrated to be sufficient to study separately stratospheric O_3 [*Scannell et al*., 2012], O_3 in the upper troposphere/lower stratosphere [*Barret et al*., 2011], and O_3 in the troposphere [*Boynard et al*., 2009; *Dufour et al*., 2010; *Wespes et al*., 2012].

3.2.2. Retrievals

[9] The IASI level 1C radiance data (1.3 million spectra per day) are distributed by EumetCast, the European Organisation for the Exploitation of Meteorological Satellites (EUMETSAT)'s Data Distribution system, and global distributions of O_3 vertical profiles are retrieved in near real time using an exclusive radiative transfer and retrieval software for the IASI O_3 product, the Fast Optimal Re-trievals on Layers for IASI (FORLI-O_3) [*Hurtmans et al*., 2012]. The FORLI radiative transfer model uses precalculated tables of absorbance of the O_3 band (1025–1075 cm^{-1}) at different pressures and temperatures. It provides profiles over 39 layers from the surface up to 39 km based on the inversion scheme of the Optimal Estimation Theory [*Rodgers*, 2000]. Details and description of FORLI are given by *Hurtmans et al*. [2012], and a comparison of performances with other retrieval algorithms is provided by *Dufour et al*. [2012]. The IASI FORLI-O_3 observations are selected for scenes with cloud coverage below 13% and with root mean square (RMS) of the spectral fit residual lower than 3.5×10^{-8} W/(cm^2 sr cm^{-1}). The O_3 a priori profile (plotted in black in Figure 1) and associated a priori covariance matrix are constructed from the McPeters/Labow/Logan climatology of O_3 profiles, which

Table 1. Cities Locations Used in This Study and the Corresponding Rural Areas (the Latter According to the Prevailing Wind Directions From the Urban Center)

	Urban Region					Rural Region			
City	Latitude Range (°N)		Longitude Range (°E)		Wind Direction	Latitude Range (°N)		Longitude Range (°E)	
Mexico City	19	19.75	−99.5	−98.75	SW	18.25	19	−100.25	−99.5
Los Angeles	33.5	34.25	−118.5	−117.75	East	33.5	34.25	−117.75	−117
Istanbul	40.75	41.5	28.75	29.5	SW	40	40.75	28	28.75
Madrid	40	40.75	−4	−3.25	East	40	40.75	−3.25	−2.5
New York	40.25	41	−74.5	−73.75	East	40.25	41	−73.75	−73
Tehran	35.25	36	51	51.75	NE	36	36.75	51.75	52.5
New Delhi	28.25	29	77	77.75	SE	27.5	28.25	77.75	78.5
Shanghai	30.75	31.5	121	121.75	SE	30	30.75	121.75	122.5
Beijing	39.5	40.25	116	116.75	SE	38.75	39.5	116.75	117.5

combines long-term satellite limb measurements and measurements from ozonesondes [*Turner*, 2004; *Hurtmans et al.*, 2012]. The constraint on the measurement has an average value of 2×10^{-8} W/(cm^2 sr cm^{-1}) which is close to the instrumental noise. Profiles and partial column products have been validated and compared with available ground-based, aircraft, O_3 sonde, and other satellite observations [*Anton et al.*, 2011; *Gazeaux et al.*, 2012; *Parrington et al.*, 2012; *Pommier et al.*, 2012]. These analyses show a good agreement in the troposphere (below 10 km) and middle stratosphere (25–40 km), where the differences are lower than 10% on average. However, a significant positive bias of about 10–26% is found between 10 and 25 km. The same bias is reported when using different retrieval algorithms [*Dufour et al.*, 2012].

[10] Interestingly, *Eremenko et al.* [2008] have shown that it was possible to study, with infrared sounders, the variation of the tropospheric O_3 column around cities in particular since high thermal contrast (the temperature difference between that of the surface and that of the first atmospheric layer), and thus more information in the boundary layer, is usually associated to the spring-summer photochemical pollution events.

[11] We plot in Figure 1 the O_3 vertical profiles (Figure 1a) and the corresponding averaging kernel functions for the merged 0–8 km columns (Figure 1b) for IASI observations recorded during January and June 2011 above the urban regions in Table 1. The vertical profiles in Figure 1a show expected higher O_3 mixing ratio values in June than in January. A significant increase in surface O_3 values between January and June is recorded for all the cities, reflecting high surface O_3 production in summer along with a high thermal contrast. In this study, we use IASI day observations of the 0–8 km tropospheric O_3 column since the information content of IASI data is shown to be higher during the day [*Clerbaux et al.*, 2009].

[12] Figure 1b shows that the averaging kernels are more sensitive to the lower troposphere in summer because of higher surface temperature and better thermal contrast, leading to a smaller contribution of the a priori profile to the retrieved profiles. We chose the 0–8 km column because it provides above 0.5 degree of freedom (the trace of the averaging kernel matrix) in the troposphere and avoids having to define a variable tropopause height, which impacts on quantifying the O_3 content in the troposphere [*Held*, 1981; *Bethan et al.*, 1996; *Hoinka*, 1997; *Reichler et al.*, 2003]: Since the cities selected for this study (see Table 1) fall in a latitude range between 19°N and 41°N, this choice thus provides a good mean to maximize the tropospheric information content while minimizing the stratospheric contamination.

[13] Figure 2 shows the latitudinal variation of the 0–8 km O_3 column over the 4 years of the study. It shows that the selected 0–8 km O_3 column captures well the signature of tropospheric O_3 at midlatitudes. The high values detected in the northern high latitudes are explained by the integration of stratospheric air into the 0–8 km column due to lower tropopause height especially in winter as well as residual stratospheric intrusions, which inject O_3-rich air below the

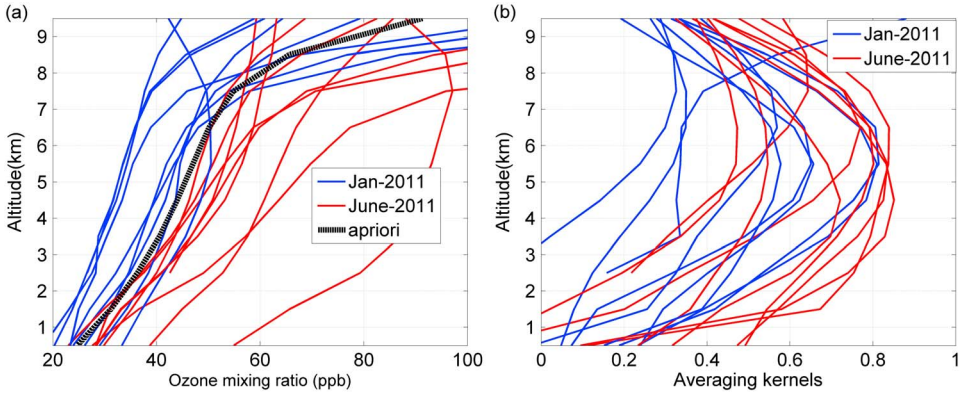

Figure 1. (a) IASI mean O_3 mixing ratio (ppb) profile for the urban cities listed in Table 1 during January 2011 (in blue) and June 2011 (in red), with the a priori profile plotted in black. (b) Averaging kernel functions for the merged 0–8 km IASI O_3 partial columns for the same locations and period. Note that some cities have altitudes > 0.

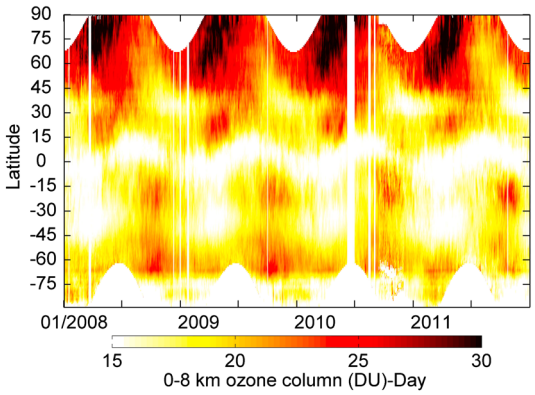

Figure 2. Latitude-time plot of the zonally averaged 0–8 km O_3 column between 2008 and 2011 for the IASI daytime observations. The white vertical lines correspond to days with no data.

8 km column during the rest of the year. High concentrations are found in the latitudes between 0°N and 45°N, where the main anthropogenic sources of tropospheric O_3 are located. On the other hand, the high values detected between 0°S and 45°S correspond likely to the biomass burning source of O_3. The figure also shows that the magnitude of the seasonal variation of the O_3 column over the period 2008–2011 is smaller for the Southern Hemisphere (SH) in comparison with the NH all year long. The highest detected O_3 values in the two hemispheres are in spring (March-April-May for NH and September-October-November for SH) for the 4 year span of 2008–2011, which coincides to the period where the intrusions from the stratosphere are the highest.

[14] The O_3 column changes according to the latitude and season. High values are especially detected in populated areas in midlatitudes due to the high emission of O_3 precursors and the photochemical production of O_3, as seen in Figure 3, which represents the monthly averaged 0–8 km O_3 column over a grid of 0.5° × 0.5°. The weakest values for the O_3 tropospheric column are observed in the high and middle latitudes of the SH as well as around the tropics, all year long except when fires occur. For the months of January and June, high O_3 concentrations are observed in high latitudes of the NH, corresponding to the stratospheric intrusion into the 0–8 km column. Photochemical production of O_3 is better highlighted during the month of June, notably in midlatitudes of the NH. The figure also shows the transport of O_3, between Northern America and Europe and between Southern America and Africa, as well as the transport of pollution from China to North America.

3.3. GOME-2 Nitrogen Dioxide Measurements

3.3.1. Instrumentation

[15] In this study, we analyze the relationship between the tropospheric O_3 columns retrieved from IASI and the GOME-2 NO_2 tropospheric columns in a polluted environment. We use GOME-2 data since it is on board the MetOp-A platform as well and offer one of the first opportunities to study the O_3-NO_2 relationship with coincident measurements. GOME-2 is a nadir-scanning UV/visible spectrometer with a swath width of 1920 km with a nominal ground pixel size of $80 \times 40\ km^2$ which allows global coverage every 1.5 days. The spectral range covered by the GOME-2 instrument is from 240 to 790 nm distributed on four main optical channels, with a spectral resolution between 0.26 and 0.51 nm [*Munro et al.*, 2006; *Valks et al.*, 2011].

3.3.2. Retrievals

[16] The operational tropospheric NO_2 product is provided by the German Aerospace Center, in the framework of the EUMETSAT O3M-SAF (Satellite Application Facility on Ozone and Atmospheric Chemistry Monitoring). The differential optical absorption spectroscopy method is used to determine NO_2 slant columns from GOME-2 (ir)radiance data in the 425–450 nm range. Initial total NO_2 columns are computed using stratospheric air mass factors, and GOME-2-derived cloud properties are used to calculate the air mass factors for scenarios in the presence of clouds. To obtain the stratospheric NO_2 component, a spatial filtering approach is used. Tropospheric air mass factors are computed using monthly averaged NO_2 profiles from the MOZART-2 (Model for OZone and Related chemical Tracers) chemistry transport model [*Valks et al.*, 2011]. Figure 4 shows the GOME-2 tropospheric NO_2 column during January and June 2011. Anthropogenic sources of NO_2 are notably detected in midlatitudes especially near populated regions with high anthropogenic activity such as in Northern America, Europe,

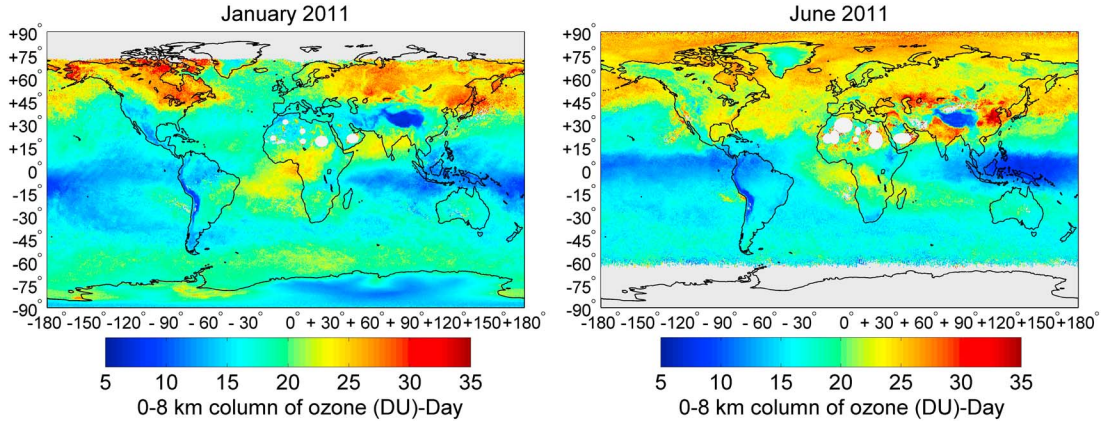

Figure 3. IASI daytime tropospheric O_3 column averaged over a grid of 0.5° × 0.5° for the months of January and June 2011. The white areas over the desert in North Africa and Saudi Arabia correspond to a filter applied on poor spectral fits, because of emissivity issues in the FORLI radiative transfer.

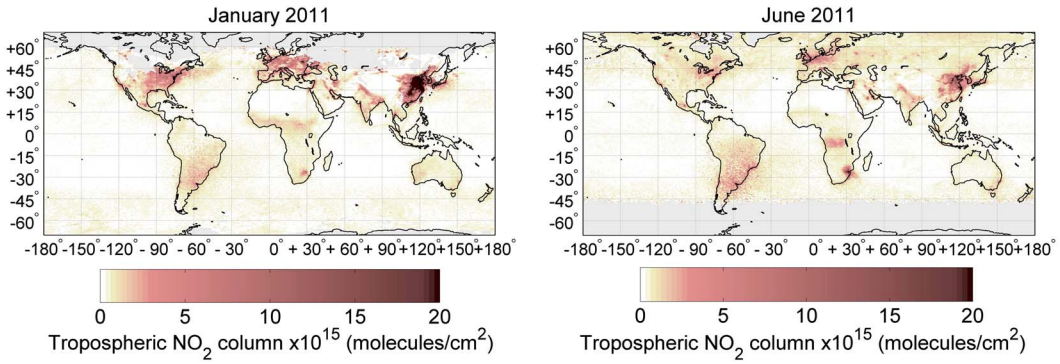

Figure 4. Monthly averaged NO_2 tropospheric column over a 0.25° × 0.25° grid for January and June 2011 as seen by GOME-2.

and Eastern Asia. In comparing the two hemispheres, we note that the NH has in both months larger NO_2 concentrations. This is also seen in Figure 5, which shows the seasonal variation over the 4 years of the study in the NH and SH. The magnitude of the tropospheric NO_2 column is larger in the NH than in the SH, all year long, for the 4 year period. The highest values are detected in winter for each hemisphere, while the lowest values are in summer. Moreover, the figure highlights the yearly increase in the NO_2 column from 2008 to 2011: While the NO_2 emission sources are expected to be reduced in industrialized countries, the rapid economic growth, in some countries such as China, is leading to an increase in the NO_2 emissions [*Richter et al.*, 2005].

4. Results

4.1. Seasonal Cycling of Ozone in Urban Regions

[17] O_3 in the troposphere shows a slower photochemistry in winter and a faster photochemistry in spring and summer [*Levy et al.*, 1985; *Klonecki and Levy*, 1997]. Figure 6 illustrates the seasonal variation of the 0–8 km O_3 column over the nine cities listed in Table 1. Both Figures 6a and 6b show a typical seasonal behavior with increasing values of O_3 in late spring (April–May) that could be associated with the transport of O_3 from the lower stratosphere to the troposphere [*Logan*, 1985]. Cities located at high latitudes are subject to larger stratospheric contamination. This can be seen in winter for the first three cities in Figure 6a: Mexico City with latitude defined between 19°N and 19.75°N has smaller winter O_3 values than Los Angeles whose location is defined between 33.5°N and 34.25°N which, in turn, has a smaller winter column than Istanbul located at a higher latitude (40.75°N–41.5°N). The second prominent peak, seen, for example, in the cities of Los Angeles and Istanbul in summer, is likely due to high anthropogenic activity. Madrid, New York, and Tehran exhibit a slightly shifted seasonal behavior, with increasing O_3 values from spring to summer and reaching its maximum in July and August where the solar activity is at its peak. Lower summertime values of O_3 such as in Los Angeles and New York could be due to the photochemical destruction of O_3, a phenomenon that is less prominent in spring than in summer [*Derwent et al.*, 1998]. Higher values are likely associated with increase in production of O_3 by its precursors and seen, for example, in Mexico City, Istanbul, Madrid, and Tehran.

[18] Figure 6b shows cities where the summer season is the rainy one, such as in New Delhi, Shanghai, and Beijing. In magnitude, the two Chinese cities presented, Shanghai and Beijing, have the highest tropospheric O_3 values, reaching 33 DU over Shanghai for the month of June 2011. The cities in Figure 6b, in particular, New Delhi and Shanghai, are characterized by a strong depletion of O_3 values (around 8–9 DU), respectively, between June on the one hand and July and August on the other hand. This could be attributed to the summer monsoon, which brings clean air masses with lower values of tropospheric O_3, as well as

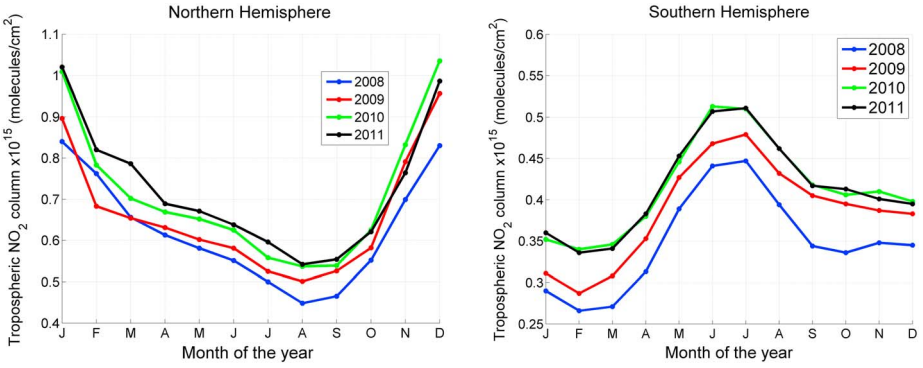

Figure 5. Seasonal variation of the tropospheric NO_2 column for the years of 2008 to 2011 in the Northern and Southern Hemispheres.

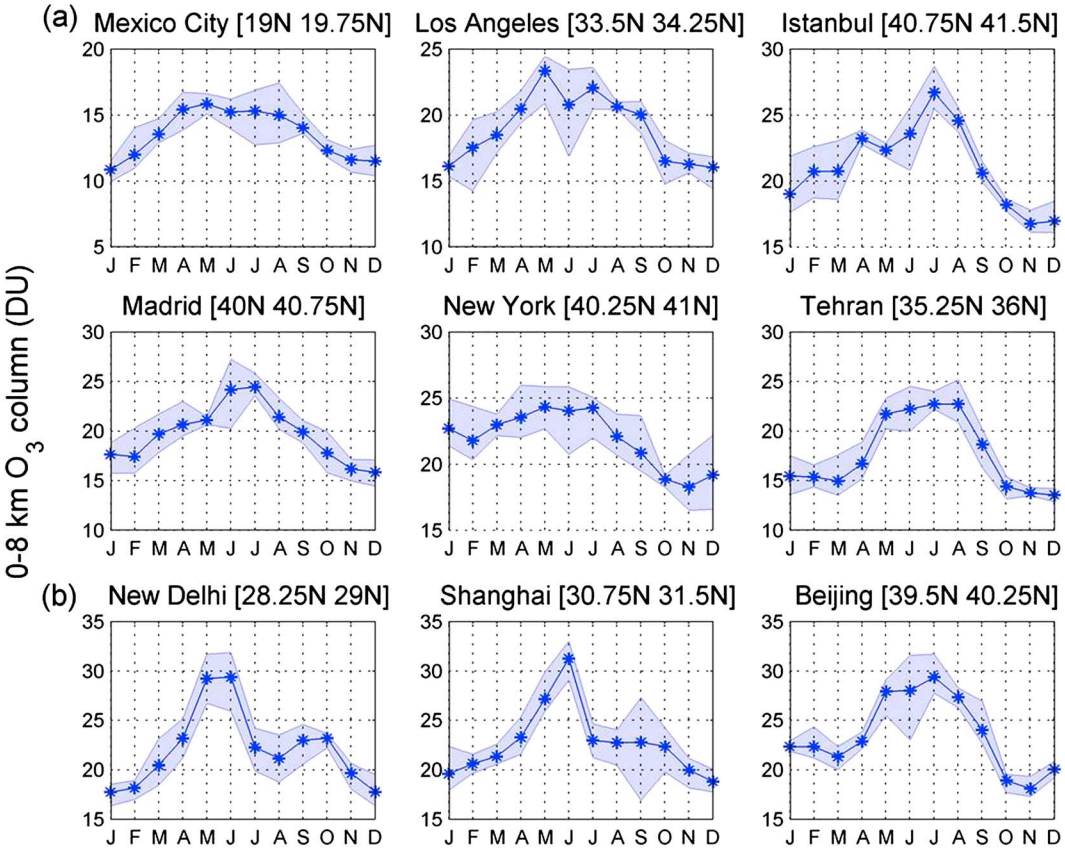

Figure 6. (a, b) Seasonal distribution of the IASI 0–8 km O_3 in selected urban regions. Results are shown for the period 2008–2011. The shaded regions show the minimum and maximum values recorded during this period.

slower photochemical activity because of clouds and the wet scavenging of O_3 precursors by rains. In New Delhi, the monsoon starts in mid-June and lasts until the end of August [*Varshney and Aggarwal*, 1992]. In Beijing and Shanghai, the East Asian summer monsoon falls in July–August and mid-June–mid-July, respectively [*Wang et al*., 2008]. The drop observed is latitude dependent: Since New Delhi and Shanghai lie closer to tropical latitudes, the intensity of the drop is larger than the one in Beijing which is, on the other hand, more susceptible to stratospheric contamination [*Dufour et al*., 2010].

4.2. Seasonal Cycling of Nitrogen Dioxide in Urban Regions

[19] The NO_2 lifetime is shorter than the one for O_3 and depends on many factors such as meteorological conditions and OH concentrations. Sunlight triggers OH production, causing NO_2 to be removed from the atmosphere [*Jacobs*, 2000; *Van der A et al*., 2006]. All cities plotted in Figure 7 show indeed minima in summer since anthropogenic NO_2 is destroyed when exposed to sunlight. On the other hand, higher values of NO_2 are expected in winter, when the days are shorter and the solar activity and OH concentrations are lower. Moreover, winter is the season with the strongest anthropogenic emissions in the NH because of heating. For all the cities, we notice that the NO_2 values are relatively higher in winter than in summer. For both tropospheric O_3 and NO_2, we notice that the columns are the highest in the economic centers of China with the highest industrial activity: Shanghai and Beijing, with average values over the 4 years of 31.2 and 29.3 DU for O_3 in June and 32.2×10^{15} and 24.5×10^{15} molecules/cm^2 for NO_2 in December, respectively. It is important to note that over highly polluted regions, most of the tropospheric NO_2 accumulates in the boundary layer [*Ma et al*., 2006], while the 0–8 km O_3 column accounts for the boundary layer contribution as well as the contribution from the long-range transport in the free troposphere.

4.3. Tropospheric Ozone and Nitrogen Dioxide in Rural Regions

[20] As explained in section 1, production of O_3 is directly related to the presence of NO_x. For low NO_x values observed in rural areas, an increase in NO_x values leads to an increase in O_3 production. This effect is better seen in Figure 8, which shows the 0–8 km O_3 column versus the tropospheric NO_2 column over rural areas surrounding the different cities of the study for the span of 2008 to 2011. The figure shows a reasonably linear behavior with Pearson correlation coefficients of 0.52 in summer and 0.61 in winter where O_3 increases as NO_2 increases. Note that the scatter in the data is likely due in part to the difference in lifetime between the two gases: NO_2 in rural areas reflects generally local sources, while O_3 is influenced by photochemical formation from NO_2, the transport from urban regions, and the long-range transport in the free troposphere that is integrated in the

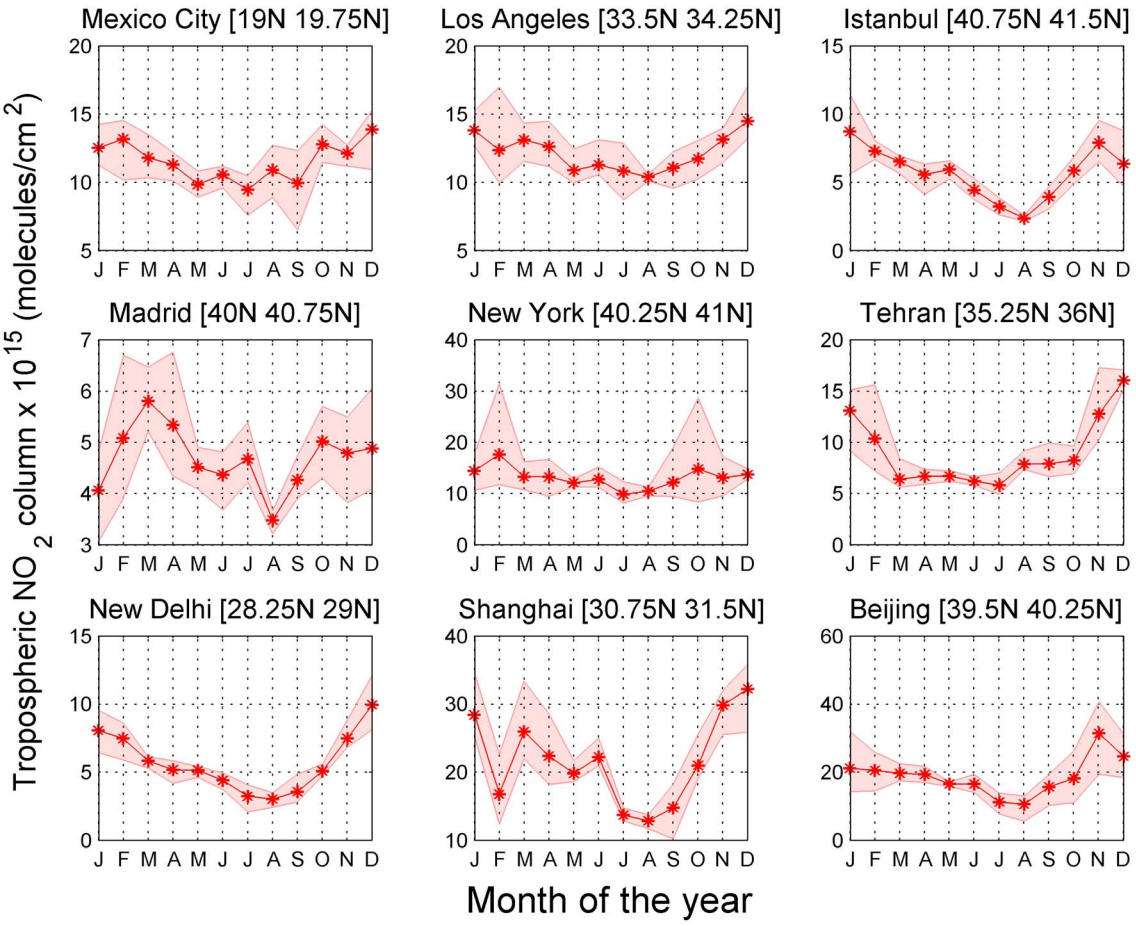

Figure 7. Same as Figure 6 but for the GOME-2 tropospheric NO_2 column.

0–8 km column, add to that the error on IASI and GOME-2 measurements and on wind directions. In fact, the approach used to determine the rural region using the prevailing wind direction may cause further uncertainties since the boundary layer winds can have strong diurnal and seasonal variations [*Lin et al.*, 2008, 2009]. The figure represents the NO_x-limited regime (section 1) since in these regions the O_3 production is partially dependent on and limited by the availability of NO_2 and increases with increasing NO_2 values.

[21] Figure 9 shows the time series from 2008 to 2011 of urban and rural tropospheric O_3 and NO_2 in the cities listed in Table 1. Over the 4 years, IASI observations (on the left) show a consistent seasonal behavior for O_3 in both urban and rural areas with maxima around spring-summer. The rural values observed are comparable to urban values and exceeding the urban values (up to 7.3 DU in May 2011 in Shanghai City) several times during the study period for all the cities. GOME-2 observations (on the right) show a

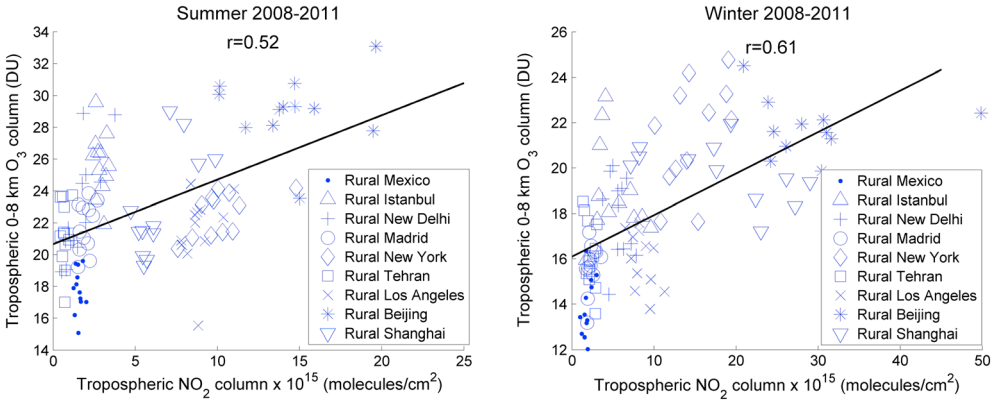

Figure 8. Summertime (1 June to 31 August) and wintertime (1 December to 28 February) O_3 and NO_2 relationship observed at rural sites for the years of 2008–2011.

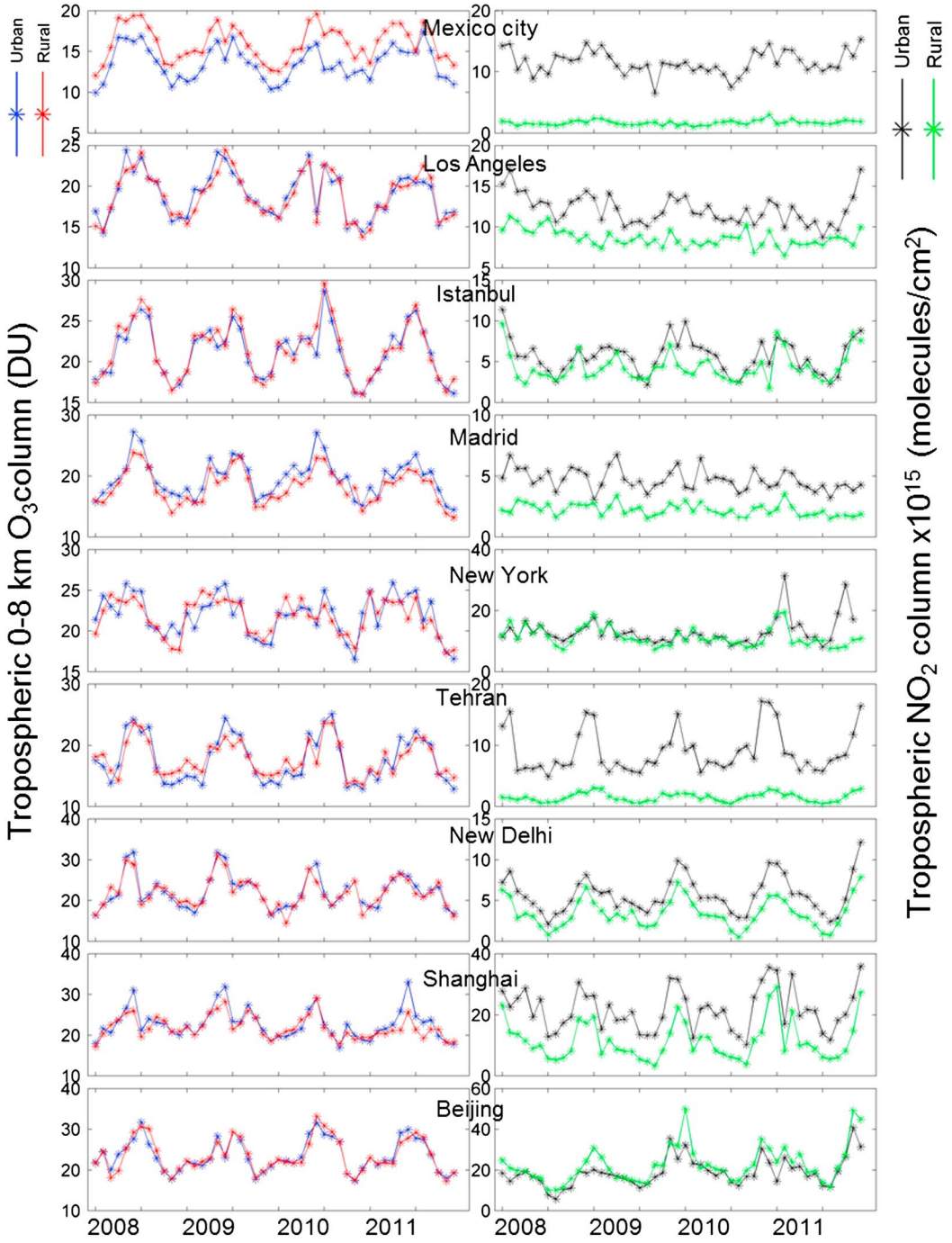

Figure 9. Time series (January 2008 to December 2011) for urban and rural tropospheric (left) O_3 and (right) NO_2 columns for the cities listed in Table 1. Tropospheric O_3 in rural areas persists, whereas the rural tropospheric NO_2 is lower.

less marked seasonal behavior for NO_2 in the nine cities, with relatively higher winter values in comparison with summer ones. During the whole study period, rural NO_2 values were observed to be lower than urban ones, except for Beijing (due perhaps to the transport by strong winds or the availability of important local emissions). The urban-rural detected difference could be due to the absence of local NO_2 sources, leading to a decrease in the rural concentrations. The largest difference is seen in New York City, where the difference reached 20.4×10^{15} molecules/cm^2 in November 2011.

4.4. Case Study of the Beijing Olympic Games of 2008

[22] In this part of the study, we focus on the analysis of the tropospheric NO_2 and O_3 columns within China by studying the case of the Olympic Games (8–24 August 2008) and the Paralympics (9–17 September 2008). Previous studies have shown, at different background sites, up to 200 km away

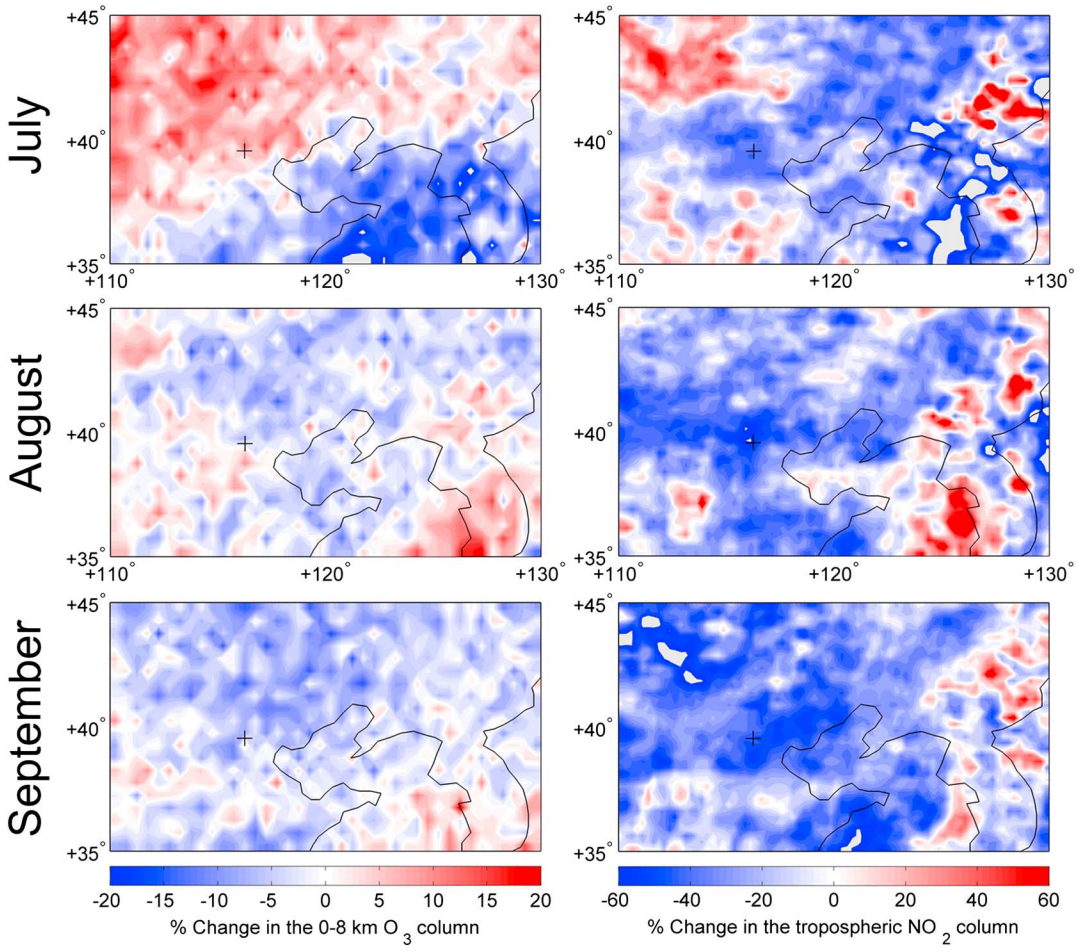

Figure 10. Percentage change in the tropospheric (left) O_3 and (right) NO_2 columns between 2008 and the average of the years 2009, 2010, and 2011. A large decrease in NO_2 is detected directly above Beijing (indicated with a cross marker), while the same effect is not detected for O_3.

from urban centers in China, a significant transport of O_3 and an enhancement in the surface O_3 [*Xu et al*., 2008]. For the past few decades, Chinese cities, such as Beijing, have been suffering from deterioration of air quality, because of the massive population and industrial growth [*Hao and Wang*, 2005]. Strict emissions control measures on vehicles and industries have been implemented between July and September 2008 for the summer Olympic and Paralympic Games in Beijing. The World Health Organization 2000 Air Quality Guidelines were used as standards for Beijing's strategy to control air quality [*United Nations Environment Programme*, 2009]. From 1 July to 20 September, these standards were applied on circulating vehicles, and traffic was reduced by 22% during the Olympics [*Wang et al*., 2009]. Strict restrictions were applied on polluting industries in Beijing and surrounding provinces, starting 8 August, the first day of the Olympics [*Li et al*., 2009]. These standards do not include surface O_3 limitations; however, because of the limitations on NO_2, O_3 values were expected to be indirectly affected. During this period, the Ozone Monitoring Instrument showed a significant decrease of around 60% in NO_2 concentrations [*Mijling et al*., 2009]. After the Olympic Games, NO_2 values were observed to return comparable to the years before [*Witte et al*., 2011]. *Worden et al*. [2012] also detected a significant decrease in CO between the summers of 2007 and 2008 using MOPITT (Measurements of Pollution in the Troposphere) satellite retrievals and WRF-Chem model (Weather Research and Forecasting model coupled with Chemistry). Upon comparing August 2006 and 2007 with the one of 2008, *Wang et al*. [2009] found a reduction of daytime O_3, SO_2, CO, and NO_y by 20%, 61%, 25%, and 21%, respectively, at a rural site 100 km downwind Beijing. *Wang et al*. [2010] reported an increase of 16% in the mixing ratio of O_3 in downtown Beijing, when comparing it with the period before the restrictions on traffic emissions. *Chou et al*. [2011] found an increase of 42.2% of the averaged mixing ratio of O_3 in August 2008 compared to the one of 2006. In this study, we compare the O_3 and NO_2 contents in summer 2008 to those of the following 3 years during the same period. Figure 10 shows the percentage difference between 2008 and the average of the years 2009, 2010, and 2011, in

Table 2. Percentage Change Between 2008 and the Average of 2009–2011 for the Area Above Beijing Whose Location Is Given in Table 1

	Percentage Change of O_3	Percentage Change of NO_2
July	+11.8	−37.7
August	−5.1	−54.3
September	−6.1	−41.3

the tropospheric NO_2 column (on the right) and the 0–8 km column of O_3 (on the left) for the different months where the restrictions were applied. It is noted that while the effect of the air quality control for NO_2 is local and direct and shows considerable decrease in the area above Beijing, up to 54.3% in August (see Table 2), the effect on the O_3 column is not similar. In fact, an increase of around 12% is observed in the month of July and a slight decrease of around 5 and 6% for the months of August and September. The increase in July could be interpreted as either the O_3 was transported by winds from nearby polluted areas such as the North China Plain [*Wang et al*., 2009, 2010] or the fact that O_3 was formed in the boundary layer since the photostationary state of the nitrogen cycle was perturbed and the reduction of the emitted NO led to an accumulation of O_3 [*Wang and Xie*, 2009].

5. Conclusions and Perspectives

[23] In this work, 4 years of tropospheric O_3 observations provided by the IASI mission are analyzed. Our results show that latitudinal and seasonal variations can be observed at the city scale. This data set was studied along with the NO_2 product provided by the GOME-2 mission flying on the same platform, over both urban and rural regions. Our data show that the assessment of tropospheric O_3 and NO_2 budgets in urban cities and rural regions is not straightforward and depends on complex photochemistry and transport processes. Tropospheric O_3 in different cities in the Northern Hemisphere shows a consistent seasonal behavior over the 4 years. Main features correspond to a peak in spring due to stratospheric intrusion and another higher one in summer due to the photochemical production of O_3 by its precursors. The seasonal variations of the 0–8 km O_3 column over New Delhi, Shanghai, and Beijing show the influence of the Asian summer monsoon that brings clean air masses from the Pacific. Tropospheric NO_2 over the same cities shows a different seasonal behavior with higher values during winter and lower values during summer. A reasonable correlation is detected in summer and winter between O_3 and NO_2. We anticipate that analyzing the effect of VOCs on the formation of O_3 would help to better explain and assess this relationship.

[24] By studying the case of the Olympic Games of summer 2008 in Beijing, we show that even when the concentration of NO_2 was well decreased in the city and its vicinity, no significant decrease of tropospheric O_3 was observed. We also suggest comparing the IASI observations with atmospheric chemistry models to see if the spatial and temporal variability agrees with the satellite observations, such as the comparison made by *Wespes et al*. [2012].

[25] More generally, the results presented in this paper, which focus on the analyses of the 0–8 km O_3 columns, further confirm that IASI is able to discriminate the tropospheric O_3 column from the total O_3. While tropospheric O_3 forecasts nowadays rely solely on regional modeling and ground-based measurements, this work is thus a new step showing that infrared satellite spectrometers, such as IASI, are capable of tracking pollution by tropospheric O_3 on a city scale and provide relevant information for air quality studies. From 2014 and onward, the FORLI-O_3 profile and partial column products will be operationally distributed through the EumetCast near real time data distribution service in the framework of the O3M-SAF project.

[26] **Acknowledgments.** IASI is a joint mission of EUMETSAT and the Centre National d'Etudes Spatiales (CNES, France). The IASI and GOME-2 L1 data are distributed in near real time by EUMETSAT through the EumetCast system distribution. The generation of the GOME-2 NO_2 operational products has been funded by the O3M-SAF project with EUMETSAT and national contributions. The authors acknowledge the French Ether atmospheric database (http://ether.ipsl.jussieu.fr) for providing the IASI L1C data. This work was undertaken under the auspices of the O3M-SAF project of the EUMETSAT. The authors would like to thank the ESA-MOST Dragon 3 Cooperation Project (ID: 10455). The French scientists are grateful to the feedback of Michel Van Roozendael, and to CNES and the Centre National de la Recherche Scientifique (CNRS) for financial support. P.-F. Coheur and C. Wespes are, respectively, Research Associate and Postdoctoral Researcher with F.R.S.-FNRS. The research in Belgium was also funded by the Belgian State Federal Office for Scientific, Technical and Cultural Affairs and the European Space Agency (ESA Prodex C4000103226).

References

Anton, M., et al. (2011), Validation of the MetOp-A total ozone data from GOME-2 and IASI using reference ground-based measurements at the Iberian peninsula, *Remote Sens. Environ.*, *115*, 1380–1386.

Barret, B., E. LeFlochmoen, B. Sauvage, E. Pavelin, M. Matricardi, and J. Cammas (2011), The detection of post-monsoon tropospheric ozone variability over south Asia using IASI data, *Atmos. Chem. Phys.*, *11*, 9,533–9,548, doi:10.5194/acp-11-9533-2011.

Bell, M., A. McDermott, S. Zeger, J. Samet, and F. Dominici (2004), Ozone and mortality in 95 US urban communities, 1987 to 2000, *JAMA*, *292*, 2372–2378.

Bell, M., R. Goldberg, C. Hogrefe, P. Kinney, K. Knowlton, B. Lynn, J. Rosenthal, C. Rosenzweig, and J. Patz (2007), Climate change, ambient ozone, and health in 50 US cities, *Clim. Change*, *82*, 61–76.

Berrisford, P., D. Dee, K. Fielding, M. Fuentes, P. Kallberg, S. Kobayashi, and S. Uppala (2009), The ERA-Interim archive. ERA report series, no.1, Tech. rep., ECMWF: Reading, UK.

Bethan, S., G. Vaughan, and S. Reid (1996), A comparison of ozone and thermal tropopause heights and the impact of tropopause definition on quantifying the ozone content of the troposphere, *Q. J. Roy. Meteorol. Soc.*, *122*, 926–944.

Boynard, A., C. Clerbaux, P.-F. Coheur, D. Hurtmans, S. Turquety, M. George, J. Hadji-Lazaro, C. Keim, and J. Meyer-Arnek (2009), Measurements of total and tropospheric ozone from IASI: Comparison with correlative satellite, ground-based and ozonesonde observations, *Atmos. Chem. Phys.*, *9*, 6255–6271.

Chappelka, A., J. Skelly, G. Somers, R. Renfro, and E. Hildebrand (1999), Mature black cherry used as a bioindicator of ozone injury, *Water Air Soil Pollut.*, *116*(1–2), 261–266.

Chou, C. C.-K., C.-Y. Tsai, C.-C. Chang, P.-H. Lin, S. C. Liu, and T. Zhu (2011), Photochemical production of ozone in Beijing during the 2008 Olympic Games, *Atmos. Chem. Phys.*, *11*, 9,825–9,837, doi:10.5194/acp-11-9825-2011.

Clarisse, L., Y. RHoni, P. Coheur, D. Hurtmans, and C. Clerbaux (2011), Thermal infrared nadir observations of 24 atmospheric gases, *Geophys. Res. Lett.*, *38*, L10802, doi:10.1029/2011GL047271.

Clerbaux, C., et al. (2009), Monitoring of atmospheric composition using the thermal infrared IASI/MetOp sounder, *Atmos. Chem. Phys.*, *9*, 6041–6054.

Coheur, P.-F., B. Barret, S. Turquety, D. Hurtmans, J. Hadji-Lazaro, and C. Clerbaux (2005), Retrieval and characterization of ozone vertical profiles from a thermal infrared nadir sounder, *J. Geophys. Res.*, *110*, D24303, doi:10.1029/2005JD005845.

Coheur, P.-F., L. Clarisse, S. Turquety, D. Hurtmans, and C. Clerbaux (2009), IASI measurements of reactive trace species in biomass burning plumes, *Atmos. Chem. Phys.*, *9*, 5655–5667.

Collins, W., D. Stevenson, C. Johnson, and R. Derwent (2000), The European regional ozone distribution and its links with the global scale for the years 1992 and 2015, *Atmos. Environ.*, *34*, 255–267.

Dee, D., et al. (2011), The ERA-Interim reanalysis: Configuration and performance of the data assimilation system, *Q. J. Roy. Meteorol. Soc.*, *137*, 553–597, doi:10.1002/qj.828.

Derwent, R., P. Simmonds, S. Seuring, and C. Dimmer (1998), Observation and interpretation of the seasonal cycles in the surface concentrations of ozone and carbon monoxide at Mace Head, Ireland from 1990 to 1994, *Atmos. Environ.*, *32*, 145–157.

Dufour, G., M. Eremenko, J. Orphal, and J.-M. Flaud (2010), IASI observations of seasonal and day-to-day variations of tropospheric ozone over three highly populated areas of China: Beijing, Shanghai, and Hong Kong, *Atmos. Chem. Phys.*, *10*, 3787–3801.

Dufour, G., M. Eremenko, A. Griesfeller, B. Barret, E. LeFlochmoen, C. Clerbaux, J. Hadji-Lazaro, P.-F. Coheur, and D. Hurtmans (2012),

Validation of three different scientific ozone products retrieved from IASI spectra using ozonesondes, *Atmos. Meas. Tech.*, *5*, 611–630.
Duncan, B., et al. (2010), Application of OMI observations to a space-based indicator of NOx and VOC controls on surface ozone formation, *Atmos. Environ.*, *44*, 2213–2223.
Ebi, K., and G. McGregor (2008), Climate change, tropospheric ozone and particulate matter, and health impacts, *Environ. Health Perspect.*, *116*, 1449–1455.
Eremenko, M., G. Dufour, G. Foret, C. Keim, J. Orphal, M. Beekmann, G. Bergametti, and J.-M. Flaud (2008), Tropospheric ozone distributions over Europe during the heat wave in July 2007 observed from infrared nadir spectra recorded by IASI, *Geophys. Res. Lett.*, *35*, L18805, doi:10.1029/2008GL034803.
Finlayson-Pitts, B., and J. Pitts (1997), Tropospheric air pollution: Ozone, airborne toxics, polycyclic aromatic hydrocarbons, and particles, *Science*, *276*, 1045–1050.
Fishman, J., and J. Larsen (1987), Distribution of total ozone and stratospheric ozone in the tropics: Implications for the distribution of tropospheric ozone, *J. Geophys. Res.*, *92*(D6), 6627–6634.
Fuhrer, J., and F. Booker (2003), Ecological issues related to ozone: Agricultural issues, *Environ. Int.*, *29*, 141–154.
Gazeaux, J., et al. (2012), Intercomparison of polar ozone profiles by IASI/MetOp sounder with 2010 Concordiasi ozonesonde observations, *Atmos. Meas. Tech.*, *5*, 7923–7944.
Hao, J., and L. Wang (2005), Improving urban air quality in China: Beijing case study, *J. Air Waste Manage. Assoc.*, *55*, 1298–1305.
Held, I. (1981), On the height of the tropopause and the static stability of the troposphere, *J. Atmos. Sci.*, *39*, 412–417.
Hoinka, K. P. (1997), The tropopause: Discovery, definition and demarcation, *Meteor. Z.*, *6*, 281–303.
Hurtmans, D., P. Coheur, C. Wespes, L. Clarisse, O. Scharf, C. Clerbaux, J. Hadji-Lazaro, M. George, and S. Turquety (2012), FORLI radiative transfer and retrieval code for IASI, *J. Quant. Spectrosc. Radiat.Transf.*, *113*, 1391–1408.
Ito, K., S. De Leon, and M. Lippmann (2005), Associations between ozone and daily mortality: Analysis and meta-analysis, *Epidemiology*, *16*, 446–457.
Jacob, D. (2000), Heterogeneous chemistry and tropospheric ozone, *Atmos. Environ.*, *34*, 2131–2159.
Jacobson, M. Z. (2012), *Air Pollution and Global Warming: History, Science, and Solutions*, 2nd ed., Cambridge Univ. Press, Cambridge.
Karnosky, D., J. Skelly, K. Percy, and A. Chappelka (2007), Perspectives regarding 50 years of research on effects of tropospheric ozone air pollution on US forests, *Environ. Pollut.*, *147*, 489–506.
Klonecki, A., and H. Levy (1997), Tropospheric chemical ozone tendencies in CO-CH4-NOy-H2O system: Their sensitivity to variations in environmental parameters and their application to a global chemistry transport model study, *J. Geophys. Res.*, *102*, 21,221–21,237.
Levy, H., J. Mahlman, and W. Moxim (1985), Tropospheric ozone: The role of transport, *J. Geophys. Res.*, *90*, 3753–3772.
Li, Y., W. Wang, H. Kan, X. Xu, and B. Chen (2009), Air quality and outpatient visits for asthma in adults during the 2008 summer Olympic Games in Beijing, *Sci. Total Environ.*, *408*(5), 1226–1227.
Lin, W., X. Xu, X. Zhang, and J. Tang (2008), Contributions of pollutants from North China Plain to surface ozone at the Shangdianzi GAW Station, *Atmos. Chem. Phys.*, *8*, 5889–5898.
Lin, W., X. Xu, B. Ge and X. Zhang (2009), Characteristics of gaseous pollutants at Gucheng, a rural site southwest of Beijing, *J. Geophys. Res.*, *144*, D00G14, doi:10.1029/2008JD010339.
Liu, X., et al. (2006), First directly retrieved global distribution of tropospheric column ozone from GOME: Comparison with the GEOS-Chem model, *J. Geophys. Res.*, *111*, D02308, doi:10.1029/2005JD006564.
Logan, J. (1985), Tropospheric ozone: Seasonal behavior, trends, and anthropogenic influence, *J. Geophys. Res.*, *90*, 10,463–10,482.
Logan, J. (1989), Ozone in rural areas of the United States, *J. Geophys. Res.*, *94*, 8511–8532.
Ma, J., A. Richter, J. Burrows, H. N. Nüß, and J. A. van Aardenne (2006), Comparison of model-simulated tropospheric NO2 over China with GOME-satellite data, *Atmos. Environ.*, *40*, 593–604.
Mijling, B., R. van der A, K. Boersma, M. Van Roozendael, I. De Smedt, and H. Kelder (2009), Reductions of NO2 detected from space during the 2008 Beijing Olympic Games, *J. Geophys. Res.*, *36*, L13801, doi:10.1029/2009GL038943.
Milford, J., A. Russell, and G. McRae (1989), A new approach to photochemical pollution control: Implications of spatial patterns in pollutant responses to reductions in nitrogen oxides and reactive organic gas emissions, *Environ. Sci. Technol.*, *23*, 1290–1301.
Milford, J., D. Gao, S. Sillman, P. Blossey, and A. Russell (1994), Total reactive nitrogen (NOy) as an indicator for the sensitivity of ozone to NOx and hydrocarbons, *J. Geophys. Res.*, *99*, 3533–3542.
Munro, R., M. Eisenger, C. Anderson, J. Callies, E. Carpaccioli, R. Lang, A. Lefebvre, Y. Livschitz, and A. Albinana (2006), GOME-2 on MetOp: From in-orbit verification to routine operations, in The 2006 EUMETSAT Meteorological Satellite Conference, Helsinki, Finland, EUMETSAT (pp. 48).
Parrington, M., et al. (2012), The influence of boreal biomass burning emissions on the distribution of tropospheric ozone over North America and the North Atlantic during 2010, *Atmos. Chem. Phys.*, *12*, 2077–2098, doi:10.5194/acp-12-2077-2012.
Pommier, M., et al. (2012), Analysis of IASI tropospheric O3 data over the Arctic during POLARCAT campaigns in 2008, *Atmos. Chem. Phys.*, *12*, 7371–7389, doi:10.5194/acp-12-7371-2012.
Reich, P. (1983), Effects of low concentrations of O3 on net photosynthesis, dark respiration, and chlorophyll contents in aging hybrid poplar leaves, *Plant Physiol.*, *73*, 291–296.
Reichler, T., M. Dameris, and R. Sausen (2003), Determining the tropopause height from gridded data, *Geophys. Res. Lett.*, *30* (2), 2042, doi:10.1029/2003GL018240.
Richter, A., J. Burrows, H. Nu, C. Granier, and U. Niemeier (2005), Increase in tropospheric nitrogen dioxide over China observed from space, *Lett. Nat.*, *437*, 129–132.
Rodgers, C. (2000), *Inverse Methods for Atmospheric Sounding: Theory and Practice*, Series on Atmospheric, Oceanic and Planetary Physics, vol. *2*, World Scientific, Hackensack.
Scannell, C., D. Hurtmans, A. Boynard, J. Hadji-Lazaro, M. George, A. Delcloo, A. Tuinder, P. F. Coheur, and C. Clerbaux (2012), Antarctic ozone hole as observed by IASI/MetOp for 2008–2010, *Atmos. Meas. Tech.*, *5*, 123–139.
Schaub, M., J. Skelly, J. Zhang, J. Ferdinand, J. Savage, R. Stevenson, D. Davis, and K. Steiner (2005), Physiological and foliar symptom response in the crowns of *Prunus serotina*, *Fraxinus americana* and *Acer rubrum* canopy trees to ambient ozone under forest conditions, *Environ. Pollut.*, *133*, 553–567.
Schoeberl, M. R., et al. (2007), A trajectory-based estimate of the tropospheric ozone column using the residual method, *J. Geophys. Res.*, *112*, D24S49, doi:10.1029/2007JD008773.
Seinfeld, J. H., and S. Pandis (2006), *Atmospheric Chemistry and Physics From Air Pollution to Climate Change*, 2nd ed., John Wiley & Sons, New York.
Sillman, S. (1999), The relation between ozone, NO*x* and hydrocarbons in urban and polluted rural environments, *Atmos. Env.*, *33*, 1821–1845.
Sillman, S., J. Logan, and S. Wofsy (1990), The sensitivity of ozone to nitrogen oxides and hydrocarbons in regional ozone episodes, *J. Geophys. Res.*, *95*, 1837–1851.
Tie, X., S. Chandra, J. R. Ziemke, C. Granier, and G. P. Brasseur (2007), Satellite measurements of tropospheric column O3 and NO2 in eastern and southeastern Asia: Comparison with a global model (MOZART-2), *J. Atmos. Chem.*, *56*, 105–125, doi:10.1007/s10874-006-9045-7.
Turner, D. (2004), Systematic errors inherent in the current modeling of the reflected downward flux term used by remote sensing models, *Appl. Opt.*, *43*(11), 2369–2383, doi:10.1364/AO.43.002369.
Turquety, S., D. Hurtmans, J. Hadji-Lazaro, P.-F. Coheur, C. Clerbaux, D. Josset, and C. Tsamalis (2009), Tracking the emission and transport of pollution from wildfires using the IASI CO retrievals: Analysis of the summer 2007 Greek fires, *Atmos. Chem. Phys.*, *9*, 4897–4913, doi:10.5194/acp-9-4897-2009.
United Nations Environment Programme. (2009), Independent environmental assessment: Beijing 2008 Olympic Games, isbn 978-92-807-2888-0.
Valks, P., G. Pinardi, A. Richter, J.-C. Lambert, N. Hao, D. Loyola, M. Van Roozendael, and S. Emmadi (2011), Operational total and tropospheric NO2 column retrieval for GOME-2, *Atmos. Meas. Tech.*, *4*, 1491–1514.
Van der A, R., D. Peters, H. Eskes, K. Boersma, M. Van Roozendael, I. De Smedt, and H. Kelder (2006), Detection of the trend and seasonal variation in tropospheric NO_2 over China., *J. Geophys. Res.*, *111*, D12317, doi:10.1029/2005JD006594.
Varshney, C., and M. Aggarwal (1992), Ozone pollution in the urban atmosphere of Delhi, *Atmos. Environ.*, *26*(3), 291–294.
Wang, T., and S. Xie (2009), Assessment of traffic-related air pollution in the urban streets before and during the 2008 Beijing Olympic Games traffic control period, *Atmos. Environ.*, *43*, 5682–5690, doi:10.1016/j.atmosenv.2009.07.034.
Wang, W., Q. Ge, J. Hao, J. Zheng, P. Zhang, and S. Sung (2008), Rainy season at Beijing and Shanghai since 1736, *J. Meteorol. Soc. Jpn*, *86*(5), 827–834.
Wang, Y., J. Hao, M. B. McElroy, J. W. Munger, H. Ma, D. Chen, and C. P. Nielsen (2009), Ozone air quality during the 2008 Beijing Olympics: Effectiveness of emission restrictions, *Atmos. Chem. Phys.*, *9*, 5237–5251.
Wang, T., et al. (2010), Air quality during the 2008 Beijing Olympics: Secondary pollutants and regional impact, *Atmos. Chem. Phys.*, *10*, 7603–7615, doi:10.5194/acp-10-7603-2010.
Wespes, C., et al. (2012), Analysis of ozone and nitric acid in spring and summer Arctic pollution using aircraft, ground-based, satellite

observations and MOZART-4 model: Source attribution and partitioning, *Atmos. Chem. Phys.*, *12*, 237–259.

Witte, J., B. Duncan, A. Douglas, T. Kurosu, K. Chance, and C. Retscher (2011), The unique OMI HCHO/NO_2 feature during the 2008 Beijing Olympics: Implications for ozone production sensitivity, *Atmos. Environ.*, *45*, 3103–3111.

Worden, H., et al. (2007), Comparisons of Tropospheric Emission Spectrometer (TES) ozone profiles to ozonesondes: Methods and initial results, *J. Geophys. Res.*, *112*, D03309, doi:10.1029/2006JD007258.

Worden, H., Y. Cheng, G. Pfister, G. Carmichael, Q. Zhang, D. Streets, M. Deeter, D. Edwards, J. Gille, and J. Worden (2012), Satellite-based estimates of reduced CO and CO_2 emissions due to traffic restrictions during the 2008 Beijing Olympics, *J. Geophys. Res.*, *39*, L14802, doi:10.1029/2012GL052395.

Xu, X., W. Lin, T. Wang, P. Yan, J. Tang, Z. Meng, and Y. Wang (2008), Long-term trend of surface ozone at a regional background station in Eastern China 1991–2006: Enhanced variability, *Atmos. Chem. Phys.*, *8*, 2595–2607.